Increasing Hydrodynamic Efficiency by Reducing Cross-Beam Energy Transfer in Direct-Drive-Implosion Experiments

D. H. Froula, I. V. Igumenshchev, D. T. Michel, D. H. Edgell, R. Follett, V. Yu. Glebov, V. N. Goncharov, J. Kwiatkowski, F. J. Marshall, P. B. Radha, W. Seka, C. Sorce, S. Stagnitto, C. Stoeckl, and T. C. Sangster

Phys. Rev. Lett. **108**, 125003 — Published 21 March 2012

DOI: 10.1103/PhysRevLett.108.125003

Increasing hydrodynamic efficiency by reducing cross-beam energy transfer in direct-drive-implosion experiments

D. H. Froula,* I. V. Igumenshchev, D. T. Michel, D. H. Edgell, R. Follett, V. Yu. Glebov, V. N. Goncharov, J. Kwiatkowski, F. J. Marshall, P. B. Radha, W. Seka, C. Sorce, S. Stagnitto, C. Stoeckl, and T. C. Sangster
Laboratory for Laser Energetics, University of Rochester, Rochester, NY 14636

A series of experiments to determining the optimum laser-beam radius by balancing the reduction of cross-beam energy transfer (CBET) with increased illumination nonuniformities shows that the hydrodynamic efficiency is increased by $\sim 35\%$, which leads to a factor of 2.6 increase in the neutron yield when the laser-spot size is reduced by 20%. Over this range, the absorption is measured to increase by 15%, resulting in a 17% increase in the implosion velocity and a 10% earlier bang time. When reducing the ratio of laser spot size to target radius below 0.8, the rms amplitude of the nonuniformities imposed by the smaller laser spots are measured to exceed 8 μm and the neutron yield saturates despite increasing absorbed energy, implosion velocity, and decreasing bang time. The results agree well with hydrodynamic simulations that include both nonlocal and CBET models.

PACS numbers: 52.38.Kd, 41.75.Jv, 52.35.Mw
Keywords:

For the direct-drive approach to inertial confinement fusion [1], laser beams deposit their energy in the coronal plasma (via inverse bremsstrahlung) and the energy is transported to the ablation surface where material rapidly expands driving the implosion. The implosion velocity of the unablated mass determines the minimum laser energy required for ignition ($E_{min} \propto v_{imp}^{-5.9}$) [2]. The implosion velocity is most efficiently driven by the central portions of the laser beams, as they propagate most normal to the target surface, where they deposit their energy close to the ablation surface. To uniformly compress the fusion capsule, the diameter of the laser beams is optimized to produce a uniform illumination while limiting the energy propagating past the target [3].

Recently cross-beam energy transfer (CBET) was identified as a mechanism for reducing the hydrodynamic coupling in direct-drive implosions by linking discrepancies in the scattered-light spectra to a lack of energy penetrating to the critical surface [4]. CBET reduces the incident energy in the central portion of the laser beams, making it possible for the incoming light to bypass the highest absorption region near the critical surface (Fig. 1), significantly reducing the hydrodynamic efficiency ($\epsilon = 1/2 m v_{imp}^2 / E_{laser}$, where m is the mass of the imploding shell, and E_{laser} is the total laser energy) [5]. Laser light in the edge of the laser beams (k_2) propagating past the target seed stimulated Brillouin scattering along the light from the opposing laser beams (k_1) that drives ion-acoustic waves (k_a) to large amplitudes. The large-amplitude ion-acoustic waves scatter light primarily from the central rays of the incident laser beams to the lower energy out going rays.

Early CBET experiments used laser beams to drive ion-acoustic waves to large amplitude by seeding the stimulated Brillouin scattering instability in planar target geometries [6–9]. More recently, CBET was identified as a mechanism for transferring significant energy within indirect drive hohlraum plasmas [10] and is used to control the symmetry of the fusion capsule at the National Ignition Facility [11].

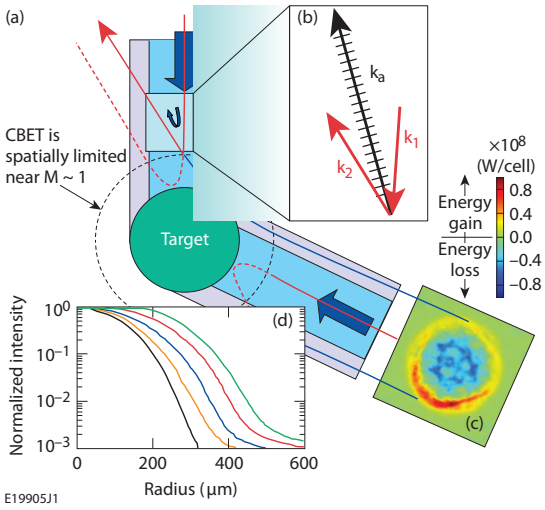

FIG. 1: (a) Light rays propagating past the target (blue) interact with light rays in the central region of another beam (red). (b) The interacting light rays seed an ion-acoustic wave near the Mach-1 surface. The ion-acoustic wave scatters light before it can penetrate deep into the target (dashed curves). (c) A calculation of the beam profile shows that energy in the central rays propagating into the target is reduced by CBET, while the energy in the edges of the beam propagating away from the target is increased. (d) The laser beam profile is measured for each defocus condition (black) $R_{beam}/R_{target} =$ 0.5, (orange) 0.65, (blue) 0.75, (red) 0.88, (green) 1.0.

In this Letter, we present the first experiments that demonstrate an increased hydrodynamic efficiency for direct-drive implosions through the mitigation of cross-beam energy transfer. By reducing the diameter of the

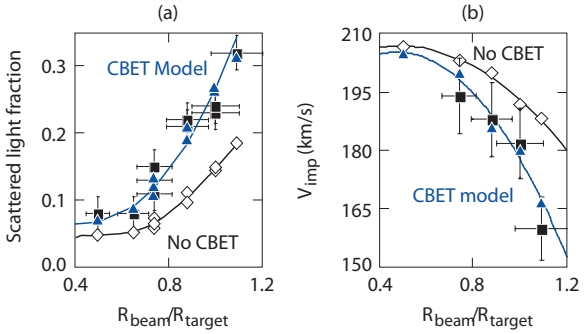

FIG. 2: The measured (a) scattered light and (b) implosion velocity is plotted as a function of the ratio between the laser-beam and target radii for the low-adiabat implosion experiments. The simulation results that include the CBET model (triangles) are in excellent agreement with the measurements. Simulations performed without the CBET model (diamonds) significantly underestimate the scattered light and overestimate the implosion velocity.

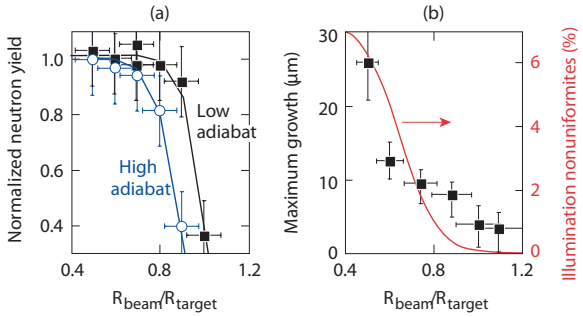

FIG. 3: The measured (a) neutron yield and (b) nonuniformity amplitude (left axis) is plotted as a function of the ratio between the laser-beam and target radii. The absorption nonuniformities calculated within the first 50 ps indicate the initial nonuniformities imposed by the laser beams (right axis). The low- (squares) and high-adiabat (circles) neutron yields are normalized to 4.7×10^9 and 5.5×10^9, respectively.

laser beams by 20%, the absorption increases by 15%, resulting in an $\sim$ 35% increase in hydrodynamic coupling as measured by a 17% increase in the implosion velocity, a 10% earlier bang time, and a factor of 2.6 increase in the neutron yield. When further reducing the laser-spot size, the rms amplitude of the nonuniformities imposed by the smaller laser spots are measured to increase from $\sim$ 3 μm to 25 μm while the neutron yield remains constant despite the increased hydrodynamic efficiency. This efficiency increase is primarily a result of the reduced CBET observed in the significant increase in the wavelength of the red-shifted scattered light when the diameter of the laser beams is reduced. These results show that an optimum laser-spot size of 0.8 to 0.9 times the target diameter will reduce CBET, increasing the hydrodynamic efficiency, resulting in a substantial increase in the neutron yield.

The experiments employed 60 ultraviolet ($\lambda_0 = 351 -$ nm) laser beams at the OMEGA Laser Facility [12]. The laser beams were smoothed by polarization smoothing (DPR) [13], smoothing by spectral dispersion (SSD) [14], and distributed phase plates (DPP) [15]. Fifty-seven elliptical phase plates were oriented with their minor axis aligned to the polarization axis of the DPR, producing a nearly round $R_{beam} = 215$ μm (95% encircled energy) laser spot at best focus. The ellipticity of these beams was measured to be less than 15%. Three round DPP's with a best focus radius of $R_{beam} = 210$ μm were used to complete the set. The radii of the laser spots were varied by defocusing the laser beams. The profiles of each defocused condition were measured on the OMEGA equivalent-target-plane diagnostic and the azimuthal averaged profiles were used in the simulations [Fig. 1(d)]. Even for the most tightly focused conditions, the laser spots have significant overlap such that the drive intensity is given by the total laser power divided by the surface area of the target.

Two pulse shapes with a maximum overlapped drive intensity of 4.5×10^{14} W-cm^{-2} were used to drive the capsules with differing hydrodynamic stability [16]. Very stable implosions driven on a high-adiabat ($\alpha \approx 5$) employed a 1-ns square pulse with a total energy on target of 10.8 kJ. A triple-picket pulse shape [17] with a 1.6-ns square drive pulse and 18 kJ of total energy was used to launch the capsule on a low-adiabat ($\alpha \approx 3$) [16]. The radius of the CH capsules was $R_{target} = 430$ μm and the thickness of the shell and D_2 gas-fill pressure were varied between 20 μm (15 atm) and 27 μm (10 atm) for the high- and low-adiabat conditions, respectively.

The total scattered energy was measured with an uncertainty of 5% using five calorimeters located around the target chamber. Scattered light collected at four locations was coupled into a 1.5-m spectrometer with a high dynamic range streak camera. The system has a 0.03-nm (FWHM) spectral resolution and a 100-ps (FWHM) temporal resolution.

The soft x-rays ($\sim$ 1 keV), produced primarily at the ablation surface, were imaged with a pinhole array ($6 - \mu m$ diameter) onto a four-strip x-ray framing camera (XRFC) with a magnification of 12 [18]. This resulted in 16 time-resolved images (4 per strip). Each image was time integrated over 40 ps. The relative timing between images is known to $<$ 10 ps after off-line calibration using 10 ps x-ray bursts produced by the Multi-TeraWatt Facility [19]. This resulted in the ability to measure the radius of the imploding shell to with an uncertainty of 7 μm and the minimum measurable variation around the average radius (nonuniformity amplitude) was ± 3 μm.

A suite of nuclear diagnostics were used to characterize the implosion performance. The neutron yield and ion temperature were measured using the 5.4-m neutron time-of-flight diagnostic (nToF) [20]. The error in the absolute neutron yield is typically $\pm$6% while the rela-

tive yield is ±3%. The absolute ion temperature was measured to within 0.5 keV and the relative shot-to-shot error is considerably smaller 0.2 keV. The neutron temporal diagnostic (NTD) [21] measured the temporal burn history of the neutrons (bang time) and had an absolute timing of < 50 ps.

Figure 2 shows that when the radius of the laser beams is reduced from $R_{beam}/R_{target} = 1.1$ to 0.85, the light that is not coupled to the target is reduced from 33% to 22% (a 15% change in absorption) leading to an increase in the implosion velocity from 160 km/s to 188 km/s [Fig. 2(b)]. This corresponds to an $\sim 35\%$ increase in the hydrodynamic efficiency. This large increase in the hydrodynamic efficiency is a factor of two larger than the increase in absorption. This is a direct result of reducing CBET which increases the energy in the central portion of the laser beams leading to more energy deposited near the critical surface.

Simulations that include both nonlocal heat transport [22] and CBET models [23] developed in the 1-dimensional hydrodynamic code LILAC [24] are in excellent agreement with the measurements shown in Fig. 2. These simulations were initiated with the measured laser pulse shapes and beam profiles [Fig. 1(d)]. A post-processor was used to investigate the 3-dimensional nature of CBET. Using the plasma parameters calculated for a single hydrodynamic time step, Fig. 1(c) shows that the energy is depleted from the center of the laser beams propagating into the Mach-1 surface while the energy is increased in the wings of the beam as they propagate out of the Mach-1 surface.

Figure 3(a) shows that the increased hydrodynamic efficiency led to more than a factor of two increase in the neutron yield while the ion temperature was measured to increase from 2.2 keV to 2.7 keV. For both the high- and low-adiabat experiments, the neutron yield saturated as a result of the nonuniformities seeded by the smaller radius laser spots. In the most-stable implosions (high adiabat), the neutron yield saturated at a smaller laser-beam radius ($R_{beam}/R_{target} \approx 0.7$) than in the high-adiabat implosions ($R_{beam}/R_{target} \approx 0.9$).

Figure 3(b) shows the amplitude of the perturbations seeded by the laser beams as determined from the soft x-ray images (Fig. 4). When the radius of the laser beams were reduced below $R_{beam}/R_{target} \simeq 0.8$, the rms amplitude of the perturbations began to exceed ~ 8 μm. These results are compared in Fig. 3(b) with the calculated initial absorption nonuniformities imposed by the laser beams. The small laser spots have a larger overlap intensity variation that provide a seed for Rayliegh Taylor growth resulting in the large measured nonuniformities. For the smallest laser spots tested, the mode with the largest amplitude corresponds to the maximum Legendre mode calculated ($\ell = 10$) from the initial absorption nonuniformities, which was a direct consequence of the geometry and the finite number of laser beams.

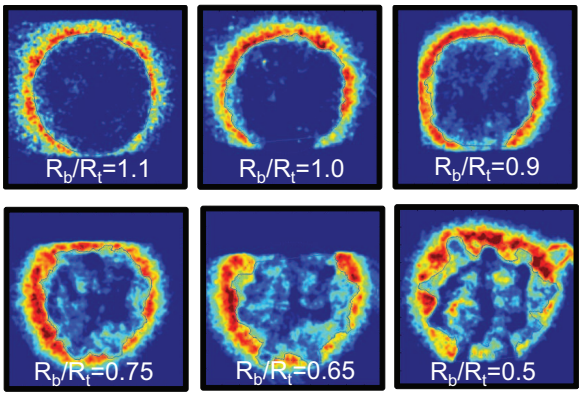

FIG. 4: The soft x-rays emitted from the ablation surface are measured by the XRFC for each defocus condition. Each image was chosen at the time of constant capsule radius $R = 175$ μm.

Figure 4 shows the XRFC images where the nonuniformities imposed by variations in laser beam illumination are clearly evident for small laser-beam radii. Post-processing of the hydrodynamic parameters shows that the bright x-ray emission from the capsules is a result of the electron temperature and density at the ablation surface. The emission is limited to a narrow $10 - \mu m$ region by the rapidly rising electron temperature and the rapidly decreasing electron density. At radii less than the ablation surface, the sharp inner emission edge closely follows the trajectory of the imploding shell while the laser beams remain on. A mode two was introduced by the instrument; the XRFC captured the left side of the image ~ 25 ps prior to the right side of the image which corresponds to a ~ 5 μm difference in radius for a typical shell velocity of 175 km/s. Mode two was removed in Fourier space from the nonuniformity calculations in Fig. 3(b). The measured shell trajectories agree well with the hydrodynamic simulations that include CBET. Figure 3(a) shows the implosion velocity measured near the end of the drive pulse (2.8 ns).

Figure 5 shows that when CBET was reduced, the red-shifted light ($\lambda > 351.2$ nm) increased, indicating that the energy in the rays that propagate closer to the critical surface was increased. Early in time, the reflected light propagates through a rapidly changing density, that reduces its effective path length, leading to a strong blue-shifted spectrum [25]. Once the coronal plasma formed (~ 1.5 ns), the light that propagates near the rapidly imploding critical surface is Doppler shifted to lower photon energies (red shifted). The simulated spectra shown in Fig. 5 agree well with all aspects of the measured spectra, indicating that not only were the general hydrodynamic profiles simulated correctly to match the observed wavelength shifts, but the detailed CBET model correctly transferred energy to match the scattered power as a function of time. This is not the case for simulations

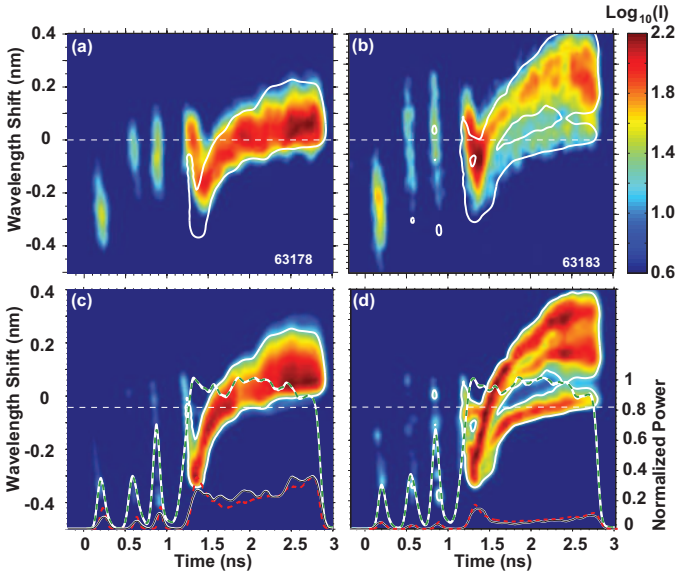

FIG. 5: The scattered light spectrum measured for the (a) maximum ($R_{beam}/R_{target} = 1.0$) and (b) minimum ($R_{beam}/R_{target} = 0.5$) CBET configuration. The spectra calculated using the nonlocal and CBET models is shown for (c) $R_{beam}/R_{target} = 1.0$ and (d) $R_{beam}/R_{target} = 0.5$. The lines that overlay the spectra are the 95% contours from the corresponding simulated spectrum. The incident laser power (white-green curve), calculated (dashed red curve) and measured (black-white curve) scattered power are shown (right axis).

that do not include a CBET model. Simulations performed without the CBET model indicate significantly more red-shifted light and overestimate the absorbed energy [Fig. 2(a)]. This leads to a predicted reduced implosion velocity and an $\sim 200-$ ps later bang time.

In summary, reducing the diameter of the laser beams by 20% in direct-drive-implosion experiments, reduces CBET, resulting in a 17% increase in the implosion velocity leading to a factor of two increase in neutron yield. Reducing CBET preferentially increases the absorption in the center of the laser beams. This results in energy being deposited closer to the critical surface, which is evident in the fact that the hydrodynamic efficiency is measured to increase by a factor of two more than the increase in absorption. This effect is verified by the increase in the wavelength of the scattered light when the diameter of the laser spots are reduced. For laser-beam diameters less than ~ 0.8 times the diameter of the target, the neutron yield remains constant despite a significant increase in absorption and implosion velocity. This saturation in neutron yield is attributed to the increase in the amplitude of the nonuniformities imposed by the laser spots that are measured to increase from $\sim 8\ \mu m$ to $25\ \mu m$. These results show that an optimum laser spot size of ~ 0.85 times the target diameter will reduce CBET, increasing the hydrodynamic efficiency, resulting in a substantial increase in the neutron yield. In general, increasing the number of laser beams, will improve the initial nonuniformities and allow this optimum ratio to be reduced.

We acknowledge the OMEGA Operations and OMAN teams whose efforts provided the unique DPP setup necessary for these results. This work was supported by the U.S. Department of Energy Office of Inertial Confinement Fusion under Cooperative Agreement No. DE-FC52-08NA28302, the University of Rochester, and the New York State Energy Research and Development Authority. The support of DOE does not constitute an endorsement by DOE of the views expressed in this article.

* Electronic address: dfroula@lle.rochester.edu

[1] J. Nuckolls *et al.*, Nature **239**, 139 (1972).
[2] M. C. Herrmann *et al.*, Nucl. Fusion **41** 99-111 (2001).
[3] J. Sanz *et al.*, Phys. Plasmas **12** 042704 (2005).
[4] W. Seka *et al.*, Phys. Plasmas **15**, 056312 (2008).
[5] I. V. Igumenshchev *et al.*, Phys. Plasmas **17**, 122708 (2010).
[6] R. K. Kirkwood *et al.*, Phys. Rev. Lett. **76**, 2065 (1996).
[7] R. K. Kirkwood *et al.*, Phys. Rev. Lett. **89**, 215003 (2002).
[8] W. Seka *et al.*, Phys. Rev. Lett. **89**, 175002 (2002).
[9] J. Myatt *et al.*, Phys. Plasmas **11**, 3394 (2004).
[10] P. Michel *et al.*, Phys. Rev. Lett. **102**, 025004 (2009).
[11] S. H. Glenzer *et al.*, Science **327**, 1228 (2010).
[12] T. Boehly *et al.*, Opt. Comm. **133**, 495 (1997).
[13] T. R. Boehly *et al.*, J. Appl. Phys. **85**, 3444 (1999).
[14] S. Skupsky *et al.*, J. Appl. Phys. **66**, 3456 (1989).
[15] Y. Lin *et al.*, Opt. Lett. **20**, 764 (1995).
[16] P. B. Radha *et al.*, Phys. Plasmas **18**, 012705 (2011).
[17] V. N. Goncharov *et al.*, Phys. Rev. Lett. **104**, 165001 (2010).
[18] D. K. Bradley *et al.*, Rev. Sci. Instr. **66**, 716 (1995).
[19] V. Bagnoud *et al.*, Opt. Lett. **30**, 1843 (2005).
[20] V. Y. Glebov *et al.*, Rev. Sci. Instr. **75**, 3559 (2004).
[21] R. A. Lerche *et al.*, Rev. Sci. Instr. **66**, 933 (1995).
[22] V. N. Goncharov *et al.*, Phys. Plasmas **15**, 056310 (2008).
[23] I. V. Igumenshchev *et al.*, To be submitted to Phys. Plasmas (2012).
[24] J. Delettrez, Can. J. Phys. **64**, 932 (1986).
[25] T. Dewandre *et al.*, Phys. Fluids **24**, 528 (1981).